A consistent spatio-temporal motion estimator for atmospheric layers

Patrick Héas, Etienne Mémin, and Nicolas Papadakis

INRIA/IRISA, Rennes, Vista Project
Campus universitaire de Beaulieu. 35000 Rennes, France
{Patrick.Heas,Etienne.Memin,Nicolas.Papadakis}@irisa.fr

Abstract. In this paper, we address the problem of estimating mesoscale dynamics of atmospheric layers from satellite image sequences. Relying on a physically sound vertical decomposition of the atmosphere into layers, we propose a dense motion estimator dedicated to the extraction of multi-layer horizontal wind fields. This estimator is expressed as the minimization of a global function including a data term and a spatio-temporal smoothness term. A robust data term relying on shallow-water mass conservation model is proposed to fit sparse observations related to each layer. A novel spatio-temporal regularizer derived from shallow-water momentum conservation model is proposed to enforce a temporal consistency of the solution along the sequence time range. These constraints are combined with a robust second-order regularizer preserving divergent and vorticity structures of the flow. In addition, a two-level motion estimation scheme is proposed to overcome the limitations of the multiresolution incremental scheme when capturing the dynamics of fine mesoscale structures. This alternative approach relies on the combination of correlation and optical-flow observations. An exhaustive evaluation of the novel method is first performed on a scalar image sequence generated by Direct Numerical Simulation of a turbulent bi-dimensional flow and then on a Meteosat infrared image sequence.

1 Introduction

The analysis of complex fluid flows behaviors is a major scientific issue. In particular, understanding atmospheric dynamics is of great importance for meteorologists interested in weather forecasting, climate prediction, singular system analysis, etc. The use of surface meteorology stations, balloons, and more recently aircraft measurements or first-generation satellite images has improved the estimation of wind fields and has been a subsequent step for a better understanding of meteorological phenomena. However, the measurements provided by the network's temporal and spatial resolutions may be insufficient for the analysis of mesoscale dynamics characterized by horizontal scales in the range of about 10-1000 km. Recently, in an effort to avoid these limitations, an increasing interest has been devoted to motion extraction from images of a new generation of geostationary satellites, with higher acquisition rates and finer spatial resolutions.

The analysis of motion in such sequences is particularly challenging due to the great deal of spatial and temporal distortions that luminance patterns exhibit in imaged atmospheric phenomena. Standard techniques from Computer Vision, originally designed for quasi rigid motions and stable salient features along time,

are not well adapted in this context. Recently, methods for fluid-dedicated dense estimation have been proposed to characterize atmospheric motion [2, 8]. Nevertheless, we will show that due to the underlying three-dimensional nature of the scene, the employed dynamical models remain unadapted to satellite observations. Furthermore, such methods may fail to accurately characterize motion associated to mesoscale structures. Thus, the design of an appropriate approach taking into account the physics of three-dimensional atmosphere dynamics constitutes a widely open domain of research. Our work is a contribution in this direction. Rather than coupling the motion vector estimation process to a complex and complete numerical meteorological circulation model, we propose to incorporate in the motion estimation scheme "image based adequate" dynamics defined as an adaptation of Navier-Stokes equations to infra-red images. The objective being in fine a three-dimensional reconstruction of atmospheric horizontal winds. Alternatively, the challenge also consists in providing accurate estimators able to tackle the motion complexity of sparse and noisy structures.

2 Related work on optical-flow estimation

The problem of wind field recovery in an image sequence $I(x, y, t)$ consists in estimating the real three-dimensional atmospheric motion from observations in the projected image plane. This problem is a complex one, for which we have only access to projected information on clouds position and spectral signatures provided by satellite observation channels. Spatial horizontal coordinates (x, y) are denoted by $\mathbf{s}$. To avoid tackling the three-dimensional wind field $\mathbf{V}(\mathbf{s}, z, t)$ reconstruction problem, up to now all the developed wind field estimation methods rely on the assumption of inexistent vertical winds and consists to estimate an average horizontal wind.

2.1 Real projected wind fields and optical-flow

The apparent motion $\mathbf{v} = (u, v)$, perceived through image intensity variations, can be computed with the standard Optical Flow Constraint (OFC):

$$I_t(\mathbf{s}, t) + \mathbf{v} \cdot \boldsymbol{\nabla} I(\mathbf{s}, t) = 0. \tag{1}$$

For image sequences showing evolving atmospheric phenomena, the brightness consistency assumption does not allow to model temporal distortions of luminance patterns caused by 3D flow transportation. For transmittance imagery of fluid flows, the so called continuity equation :

$$\frac{1}{\rho}\frac{D\rho}{Dt} + \boldsymbol{\nabla}.\mathbf{V} = 0, \tag{2}$$

may be derived from the 3D mass conservation law, where ρ denotes a three-dimensional density function. In this case, an apparent motion $\mathbf{v}$ is redefined as a density-weighted average of the original three-dimensional horizontal velocity field. For the case of a null motion on the boundary planes, in [3], the author showed that the integration of Eq.2 leads to a 2D Integrated Continuity Equation (ICE):

$$\Big(\int \rho dz\Big)_t + \mathbf{v}.\boldsymbol{\nabla}\Big(\int \rho dz\Big) + \Big(\int \rho dz\Big)\mathrm{div}(\mathbf{v}) = 0, \tag{3}$$

Unlike the OFC, such models can compensates mass departures observed in the image plan by associating two-dimensional divergence to brightness variations. By time integration, an equivalent non-linear formulation can be recovered [2] :

$$\Big(\int \rho dz\Big)(\mathbf{s}+\mathbf{v}, t+1)\exp \operatorname{div}(\mathbf{v}) - \Big(\int \rho dz\Big)(\mathbf{s}, t) = 0. \tag{4}$$

The image formation model for satellite infrared imagery is slightly different. In [2], the authors have directly assumed the unrealistic hypothesis that infrared pixel values I were proportional to density integrals : $I \propto \int \rho dz$. In [16], the authors proposed an inversely proportional approximation for infrared measurements : $I \propto (\int \rho dz)^{-1}$.

2.2 Regularization schemes and minimization issues

The previous formulations of Eq. 1, 3 and 4 can not be used alone, as they provide only one equation for two unknowns at each spatio-temporal locations $(\mathbf{s}, t)$. To deal with this problem, the most common assumption consists in enforcing spatial and temporal local coherence.

Disjoint local smoothing methods considers neighborhoods centered at pixel locations. An independent parametric field is locally estimated on each of these supports. In the the work of *Lucas and Kanade* [7], relying on the OFC equation, motion which is assumed to be locally constant is estimated using a standard linear least square approach. In meteorology, classical approaches are Euclidean correlation-based matchings, which corresponds to the OFC constraint associated to a locally constant field and a $\boldsymbol{L}^2$ norm [6, 10, 12]. On the one hand, these methods are fast and are able to estimate large displacement of fine structures. On the other hand, they present the drawback to be sensitive to noise and inefficient in the case of weak intensity gradients. Moreover, estimation with these approaches is prone to erroneous spatial variability and results in the estimation of sparse and possibly incoherent vector fields.

Globalized smoothing schemes can be used to overcome the previous limitations. These methods model spatio-temporal dependencies on the complete image domain. Thus, dense velocity fields are estimated even in the case of noisy and low contrasted observations. More precisely, the motion estimation problem is defined as the global minimization of a energy function composed of two components :

$$J(\mathbf{v}, I) = J_d(\mathbf{v}, I) + \alpha J_r(\mathbf{v}). \tag{5}$$

The first component $J_d(\mathbf{v}, I)$ called the data term, expresses the constraint linking unknowns to observations while the second component $J_r(\mathbf{v})$, called the regularization term, enforces the solution to follow some smoothness properties. In the previous expression, $\alpha > 0$ denotes a parameter controlling the balance between the smoothness and the global adequacy to the observation model. In this framework, Horn and Schunck [5] first introduced a data term related to the OFC equation and a first-order regularization of the two spatial components u and v of velocity field $\mathbf{v}$. In the case of transmittance imagery of fluid flows, $I = \int \rho dz$, and using the previously defined ICE model (Eq.3) leads to the

functional :

$$J_d(\mathbf{v}, I) = \int_\Omega \left(I_t(\mathbf{s}) + \mathbf{v}(\mathbf{s}) \cdot \boldsymbol{\nabla} I(\mathbf{s}) + I(\mathbf{s}) \mathrm{div}(\mathbf{v}(\mathbf{s}))\right)^2 d\mathbf{s}. \tag{6}$$

Moreover, it can be demonstrated that a first order regularization is not adapted as it favors the estimation of velocity fields with low divergence and low vorticity. A second order regularization on the vorticity and the divergence of the defined motion field can advantageously be consider as proposed in [11][2][15] :

$$J_r(\mathbf{v}) = \int_\Omega \parallel \boldsymbol{\nabla} curl \mathbf{v}(\mathbf{s}) \parallel^2 + \parallel \boldsymbol{\nabla} div \mathbf{v}(\mathbf{s}) \parallel^2 d\mathbf{s}. \tag{7}$$

Instead of relying on a $\boldsymbol{L}^2$ norm, robust penalty function ϕ_d may be introduced in the data term for attenuating the effect of observations deviating significantly from the ICE constraint [1]. Similarly, a robust penalty function ϕ_r can be used if one wants to handle implicitly the spatial discontinuities of the vorticity and divergence maps. In the image plan, these discontinuities are nevertheless difficult to relate to abrupt variations of clouds height . Moreover, layers clouds form unconnected regions which should interact during the motion estimation process.

OFC or ICE model rely on the assumption that the intensity function can be locally efficiently approximated by a linear function. Since the larger the displacement the more narrow the linearity domain, large displacements are difficult to recover directly. The multiresolution approach is a common way to overcome this limitation. However, since the multiresolution schemes estimates principal component displacements only at coarse resolutions where small photometric structures are rubbed out, this approach enables the characterization of large displacements of small structures only in the case when their motion are close enough to the principal component's one. This is often not the case for a multi-layered atmosphere.

3 Dense motion estimator dedicated to atmospheric layers

3.1 Dynamical model for layers

The ICE model relies on strong assumptions in the case of satellite infrared imagery. However, it has been demonstrated that this approach is well suited for an image sequence of transmittance measurements.

Since there is a lack of information induced by projection in an image plane, several hypothesis are necessary to tackle the reconstruction problem. We assume that the lower part of the atmosphere is in hydrostatic equilibrium. This assumption provides an excellent approximation for the vertical dependence of the pressure field and enables a layer decomposition of the three-dimensional space [4]. Let us denote pressure and gravity respectively by p and g. By the vertical integration of the hydrostatic equation $-\rho g = \frac{dp}{dz}$, density integrals are linked to pressure differences :

$$g \int_{z_b}^{z_t} \rho \, dz = p(z_b) - p(z_t). \tag{8}$$

where the lower and higher boundary functions are denoted by z_b and z_t. The problem is thus moved on to the derivation of pressure difference maps from infrared images for each layer.
Let us first explain how the layer are dissociated. The membership of clouds to a layer is determined by a height classification map routinely provided by the EUMETSAT consortium, the European agency which manages the Meteosat satellite data. We denote by C^k a class corresponding to the k-th layer in between the altimetric interval function $[z_b^k, z_t^k]$. Note that the top of cloud pressure image denoted by $p_{\bigcup_k}$ is composed of segments of top of clouds pressure functions $p(z_t^k)$ related to the different layers. That is to say :

$$p_{\bigcup_k} = \bigcup_k p(z_t^k, \mathbf{s}); \;\; \mathbf{s} \in C^k. \tag{9}$$

Sparse pressure maps of the layers upper boundaries are computed from infrared images as described in [13]. As in satellite images, clouds lower boundaries are always occluded, we approximate the missing pressure observations $p(z_b^k)$ by an average pressure value observed on top of the underneath layer. Finally, for the k-th layer, we define image observations as the pressure difference :

$$p(z_b^k) - p_{\bigcup_k}, = h^k \begin{cases} = g \int_{z_b^k}^{z_t^k} \rho \, dz \;\; if \; \mathbf{s} \in C^k \\ \neq g \int_{z_b^k}^{z_t^k} \rho \, dz \;\; if \; \mathbf{s} \in \bar{C}^k. \end{cases} \tag{10}$$

Thus, if we neglect vertical wind on layer boundaries, the ICE model of Eq.3 holds for observations h^k on regions of C^k, and constitute a physically sound model for motion estimation of atmospheric layers evolving independently. $\forall k \in [0, K]$:

$$\frac{\partial h^k}{\partial t} + \mathbf{v} \cdot \boldsymbol{\nabla} h^k + h^k \mathrm{div}(\mathbf{v}) = 0, \tag{11}$$

where K is the highest layer index and $\mathbf{v}$ corresponds to the density-weighted average horizontal wind related to the k-th layer. Note that as vertical wind on the layer boundaries has been neglected, this model assumes independent layer motion. Due to the hydrostatic relation, h^k may be viewed as an atmospheric layer thickness function if we assume shallow layers and thus neglect density variations : $h^k = g\rho(z_b^k - z_t^k)$. The ICE equation then corresponds to shallow-water mass conservation model [4].

3.2 Robust estimator for sparse observations

Relatively to the different layers, true pressure differences are sparsely observed only in the presence of clouds. A dense estimator dedicated to layer motion should consider simultaneously all cloudy regions belonging to a given layer while discarding the influence of other clouds. For the k-th layer, we previously remarked that outside the class 'C^k', the so defined pressure difference h^k is not relevant of the k-th layer thickness. Thus, we propose to introduce in Eq.4 a masking operator on unreliable observations. We denote by $\mathbf{M}_{\mathbf{s} \in C^k}$ the operator which is identity if pixel belongs to the class, and which returns otherwise a fixed

value out of the range taken by h^k. Thus, applying this new masking operator in Eq.4, we obtain the robust data term $J_d(\mathbf{v}, h^k)$:

$$\int_\Omega \phi_d\{exp\mathrm{div}(\tilde{\mathbf{v}}(\mathbf{s}))([\tilde{h}^k(\mathbf{s})\boldsymbol{\nabla}\mathrm{div}(\tilde{\mathbf{v}}(\mathbf{s}))+\boldsymbol{\nabla}\tilde{h}^k(\mathbf{s})]^T\mathbf{v}'(\mathbf{s})+\tilde{h}^k(\mathbf{s}))-\mathbf{M}_{\mathbf{s}\in C^k}(h^k(\mathbf{s}))\}d\mathbf{s}, \quad (12)$$

where $\mathbf{v}$ corresponds to the density-weighted average horizontal wind related to the k-th layer. The div-curl regularization term (Eq.7) is conserved. The masking procedure together with the use of robust penalty function on the data term allows to discard implicitly the erroneous observation from the estimation process. It is important to outline that, for the k-th layer, the method provides dense motion fields and areas outside class 'C^k' correspond to an interpolated wind field. Nevertheless, let us point out that in the case of very sparse observations and large displacements, robust estimation becomes unstable and may lead to erroneous minima. Such limitations will be overcome in the following.

4 A two level decomposition for mesoscale motion estimation

In order to enhance the estimation accuracy, a collection of correlation-based vectors $\mathbf{v}_c$ is introduced as sparse constraints in a differential estimation scheme for the recovery of a dense displacement field. Contrary to the classical multiresolution approach, this new technique enables to deal with the large displacements of small structures as it relies on a unique representation of the full resolution image. Moreover, in order to preserve spatio-temporal consistency of displacement estimates, we propose to incorporate in the estimation scheme an *a priori* physical knowledge on fluid dynamical evolution. A dense displacement field $\mathbf{v}_p$ is predicted by time integration of a simplified Navier-Stokes dynamical model. The propagated field is then introduced in the estimation process as a spatio-temporal regularizer. Keeping notations of section 2.2, a new functional is defined for the estimation of variable $\mathbf{v}$

$$J(\mathbf{v}) = J_d(\mathbf{v}, h^k) + \gamma J_c(\mathbf{v}, \mathbf{v}_c) + \alpha J_r(\mathbf{v}) + \beta J_p(\mathbf{v}, \mathbf{v}_p), \quad (13)$$

where $J_c(.)$, $J_p(.)$ are energy functions respectively constraining displacements $\mathbf{v}$ to be close to a sparse correlation-based vector field $\mathbf{v}_c$ and to be consistent with a physically sound prediction $\mathbf{v}_p$ relying on Navier-Stokes equations. In the previous expression, γ and β denote weighting factors. Functionals $J_c(.)$ and $J_p(.)$ will be further detailed in the following.

The displacement field $\mathbf{v}$ is decomposed into a large displacement field $\bar{\mathbf{v}}$ and an additive small displacement field $\tilde{\mathbf{v}}$. The optimization problem is conducted sequentially. Here, an analogous version of the alternate multigrid minimization scheme proposed in [2] has been implemented.

Note that in the case $\alpha, \beta, \gamma \gg 1$, the energy minimization leads to a large displacement field which can be seen as a physically sound spatio-temporal interpolation of the correlation-based vectors.

4.1 Variational approach for a correlation/optical-flow collaboration

In order to obtain a dense estimation of displacements fitting a sparse correlation-based displacement field, we define a functional where the i^{th} correlation-based

vector $\mathbf{v}_c^i = (u^i, v^i)$ located at the point $\mathbf{s}^i = (x^i, y^i)$ influences his neighborhood according to a shifted bi-dimensional Gaussian law $\mathcal{N}^i(\mathbf{s}^i - \mathbf{s})$ of variance σ related to the correlation window influence

$$J_c(\mathbf{v}, \mathbf{v}_c) = \int_\Omega \mathbf{M}_{\mathbf{s}\in C^k} \left(\sum_{i=1}^{K} g^i \mathcal{N}^i(\mathbf{s}^i - \mathbf{s}) \phi_c\{\mathbf{v}_c^i - \mathbf{v}(\mathbf{s})\} \right) d\mathbf{s}, \tag{14}$$

where ϕ_c is a robust penalty function similar to the one attached to the data term. In the previous expression, g^i denote confidence factors. We choose, to define them according to the dissimilarity function. The masking operator $\mathbf{M}_{\mathbf{s}\in C^k}()$ was introduced as the correlation/optical-flow collaboration is not possible in regions with no image observations.

4.2 Spatio-temporal regularization

The functional $J_p(.)$ aims at constraining a motion field to be consistent with a physically predicted wind field. We simply define this functional as a quadratic distance between the estimate field $\mathbf{v}$ and the dense propagated field $\mathbf{v}_p$:

$$J_p(\bar{\mathbf{v}}, \mathbf{v}_p) = \int_\Omega \parallel \mathbf{v}_p(\mathbf{s}) - \mathbf{v}(\mathbf{s}) \parallel^2 d\mathbf{s}. \tag{15}$$

This approach constitutes an alternative to the spatio-temporal regularizer defined in [14] and is to some extend similar to the temporal constrain introduced in [9]. Our propagation model includes a bi-dimensional divergence component which is equal to zero only for incompressible bi-dimensional flows. As it is detailed below, our approach extends [9] to the spatio-temporal smoothing of the full velocity field in the case of three-dimensional geophysical flows driven by a shallow-water evolution law.

Dynamical models describing wind field evolution are needed here for the prediction at time $t+1$ of a sound field $\mathbf{v}_p$ using the previous motion estimation $\mathbf{v}$ performed for the k-th layer between time $t-1$ and t. As atmosphere evolution is governed by fluid flows laws, we rely on Navier-Stokes equations in order to derive simplified dynamical models adapted to short time propagation of layer mesoscale motions. A scale analysis of the horizontal momentum equations showed that the Coriolis, the curvature terms and the friction forces are in this case negligible. Denoting by ν a turbulent viscosity coefficient, imposing incompressibility in the hydrostatic relation, and adding the mass conservation model of Eq.11, we form the complete shallow-water equation system :

$$\begin{cases} \mathbf{v}_t + \mathbf{v} \cdot \boldsymbol{\nabla}(\mathbf{v}) + \frac{1}{\rho_0} \boldsymbol{\nabla} h^k = \nu \Delta(\mathbf{v}), \\ h_t^k + \mathbf{v} \cdot \boldsymbol{\nabla} h^k + h^k \zeta = 0, \end{cases} \tag{16}$$

with the notations $\boldsymbol{\nabla}(\mathbf{v}) = (\boldsymbol{\nabla} u, \boldsymbol{\nabla} v)^T$ and $\Delta(\mathbf{v}) = \boldsymbol{\nabla} \cdot \boldsymbol{\nabla}(\mathbf{v})$. Denoting the vorticity by $\xi = \mathrm{curl}(\mathbf{v})$ and the divergence by $\zeta = \mathrm{div}(\mathbf{v})$, the previous system may be expressed in a vorticity-divergence form :

$$\begin{cases} \xi_t + \mathbf{v} \cdot \boldsymbol{\nabla} \xi + \xi \zeta = \nu \Delta \xi, \\ \zeta_t + \mathbf{v} \cdot \boldsymbol{\nabla} \zeta + \zeta^2 = 2det(J(u, v)) - \frac{\Delta h^k}{\rho_0} + \nu \Delta \zeta, \\ h_t^k + \mathbf{v} \cdot \boldsymbol{\nabla} h^k + h^k \zeta = 0, \end{cases} \tag{17}$$

where $J(.)$ is the Jacobian operator. The dynamical model predict the evolution of 3 variables which may depend on each others. One of the major difficulties is

induced by the fact that variable h^k is derived only for cloudy regions corresponding to the k-th layer. Therefore, variable h^k, and thus all unknowns, can only be propagated on a sparse spatial support. However, in opposition to the classical formulation, the vorticity-divergence equations provide a dynamical model for which the vorticity evolution is independent of variable h^k and for which the divergence evolution depends only weakly on variable h^k (up to a constant). Based on the assumption that divergence is weak almost everywhere and assimilable to noise, we propose to simplify the divergence dynamical model in order to make it independent of variable h^k. Divergence ζ is assumed to be driven by a Gaussian random function with stationary increments (i.e. a standard Brownian motion). As a consequence, divergence expectation asymptotically obeys to a heat equation of diffusion coefficient ν. The simplified vorticity-divergence model reads:

$$\begin{cases} \xi_t + \mathbf{v} \cdot \boldsymbol{\nabla}\xi + \xi\zeta = \nu\Delta\xi, \\ \zeta_t = \nu\Delta\zeta. \end{cases} \tag{18}$$

The curl and divergence completely determine the underlying 2D velocity field and the current velocity estimate can be recovered from these quantities up to a laminar flow. Indeed, the Helmholtz decomposition of the field into a sum of gradients of two potential functions is expressed as $\mathbf{v} = \boldsymbol{\nabla} \times \Psi + \boldsymbol{\nabla}\Phi + \mathbf{v}_{har}$, where $\mathbf{v}_{har}$ is an harmonic transportation part ($div\mathbf{v}_{har} = curl\mathbf{v}_{har} = 0$) of the field $\mathbf{v}$ and where the stream function Ψ and the velocity potential Φ correspond to the solenoidal and the irrotationnal part of the field. The latter are linked to divergence and vorticity through two Poisson equations. Expressing the solution of both equations as a convolution product with the 2D Green kernel G associated to the Laplacian operator: $\Psi = G * \xi$, $\Phi = G * \zeta$, the whole velocity field can be recovered with the equation :

$$\mathbf{v} = \boldsymbol{\nabla} \times (G * \xi) + \boldsymbol{\nabla}(G * \zeta) + \mathbf{v}_{har}, \tag{19}$$

which can be efficiently solved in the Fourier domain.

Let us sum up this prediction process. The vorticity and the divergence fields are developed from t to $t+1$ using a discretized form of Eq.18 and time increments Δt. After each time increment, assuming $\mathbf{v}_{har}$ constant between the same time interval, Eq.19 is used to update the velocity $\mathbf{v}$ needed by Eq.18, with the current vorticity and divergence estimates. Classical centered finite difference schemes are used for the curl and divergence discretization. To avoid instability, a semi-implicit time discretization scheme is used to integrate forward Eq.18. To solve the linear system associated to the semi-implicit discretization scheme, the matrix has been constrained to to be diagonally dominant. Finally, the dynamical model time integration is done independently for each layer. This procedure results in a predicted average horizontal wind field $\mathbf{v}_p$ related to each layer.

5 Experimental evaluation

For an exhaustive evaluation, we first propose to rely on a simulated flow. A Direct Numerical Simulation (DNS) of a 2D, incompressible, and highly turbulent flow has been used to generated an image sequence depicting the motion of a continuous scalar field. The sequence of scalar images of 256 by 256 pixels together with the true vector fields generated by the DNS were provided by the

laboratory of fluid mechanics of *Cemagref (center of Rennes, France)*. The thickness conservation model reduces in this 2D case to the classical OFC data model. Note that as divergence vanishes, the spatio-temporal regularization constrains only vorticity to be coherent in time.

In order to experiment our method with correlation-based vectors with different noise level, the correlation-based vectors have been substituted by DNS vectors contaminated by an additive Gaussian noise. As correlation techniques only operate on contrasted regions, vector constraints were attached to regions with sufficient gradient. To be realistic with correlation measurements, DNS vectors have been sub-sampled in those regions. DNS velocity vectors which have been selected as non-noisy correlation measurements are presented in fig.1. They are superimposed to the scalar image. Based on the non-noisy correlation con-

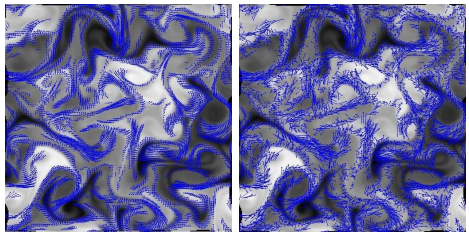

Fig. 1. ***Velocity constraints and fluid imagery for a bi-dimensional flow.*** *Left: velocity vectors provided by the DNS which have been selected as constraints are superimposed on the image. Right: Gaussian noise* $\mathcal{N}(0,1)$ *has been added to these vectors.*

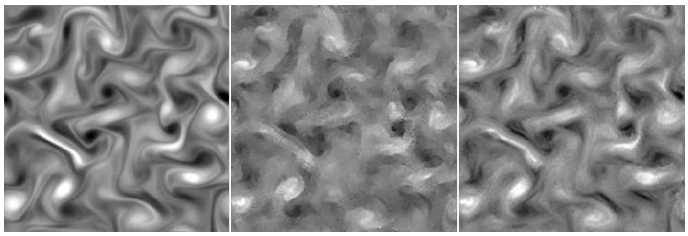

Fig. 2. ***Comparison on the image domain of multiresolution and collaborative schemes in the case of a bi-dimensional flow.*** *Left: vorticity provided by the DNS. Center: vorticity estimation by the fluid flow dedicated multiresolution approach of [2].Right: vorticity estimation after the second level of the collaborative scheme.*

straints defined previously, we first compare our two-level collaborative scheme to the fluid flow dedicated multiresolution approach described in [2]. In Fig.2, it clearly appears that the multiresolution approach hardly estimates fine turbulent structure while the collaborative method manages to recover most of the vorticity field structures. Indeed, in scalar imagery, low contrast regions correspond to high vorticity areas. Thus, the multiresolution technique suffers from a lack of information in those crucial regions. And, incorporating motion constraints in contrast areas around vortices reduces the degree of freedom of the solution and thus, considerably enhances the estimated motion field. In order to evaluate the robustness of the collaborative method to inaccurate constraints, Gaussian noise

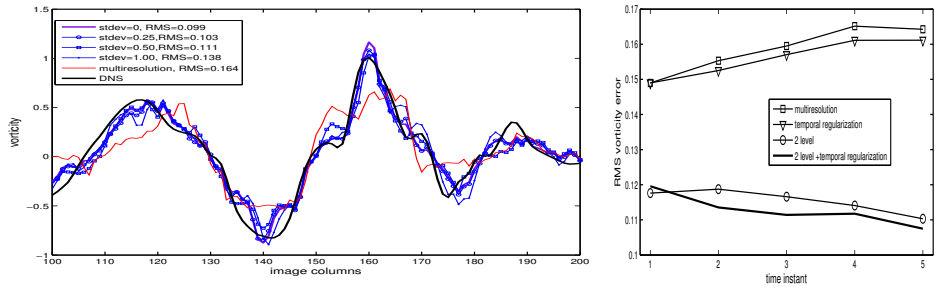

Fig. 3. ***Influence of noise and spatio-temporal regularization.*** *Left: for increasing noise, vorticity estimates on a slice of the image and global RMS vorticity error in comparison to the multiresolution approach. Right: RMS vorticity errors on five consecutive estimations for the multiresolution approach, the collaborative scheme constrained by noisy correlation vectors combined or not with spatio-temporal regularization.*

of zero mean and increasing variance has been added to the true velocity vectors provided by the DNS. Constraint examples are displayed in Fig.1. In Fig.3, we can visually inspect the influence of noise on the estimated solution for a particular horizontal slice of the image and for the global image domain by referring to RMS errors on vorticity values. It clearly appears that, even in presence of noise, motion estimation is better achieved by our collaborative scheme than by a classical multiresolution approach. Spatio-temporal regularization benefits which are assessed for both, multiresolution and collaborative methods, are shown in Fig.3.

We then turned to qualitative comparisons on a real meteorological image sequence. The benchmark data was composed by a sequence of 18 Meteosat Second Generation (MSG) images, showing thermal infrared radiation at a wavelength of 10.8 mm. The 512 x 512 pixel images cover an area over the North-Atlantic Ocean, off the Iberian peninsula, during part of one day (5-June-2004), at a rate of one image every 15 minutes. The spatial resolution is 3 kilometers at the center of the whole Earth image disk. Clouds from a cloud-classification product derived from MSG images by the operational centre EUMETSAT, are used to segment images into 3 broad layers, at low, intermediate and high altitude. This 3 layers decomposition is imposed by the EUMETSAT classification. Applying the methodology previously described, pressure difference images were derived for these 3 layers.

Trajectories reconstructed by a Runge-Kutta integration method [2] from the estimated wind fields provide a practical visualization tool to assess the quality of the estimation in time and space.

The enhancements brought by the collaborative estimation scheme for the recovery of a wind field related to the highest layer is shown in Fig.4. It can be noticed in this comparative figure that the introduction of spatio-temporal constraints smooths trajectory discontinuities and, together with the introduction of correlation constraints, propagate motion in regions where observations are missing. Using the collaborative framework and the spatio-temporal regularizer,

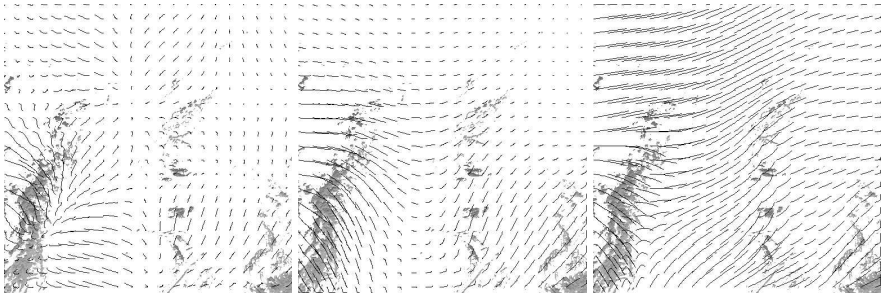

Fig. 4. ***Collaborative approach and spatio-temporal regularization influence*** *on the estimation of wind field for the highest layer. Trajectories reconstruction for an estimation scheme without (left) and with (center) spatio-temporal regularization. Trajectories reconstruction for the two-level collaborative estimation scheme with spatio-temporal regularization (right).*

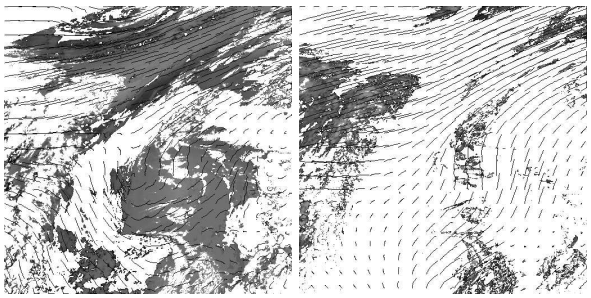

Fig. 5. ***Middle layer and lower layer trajectories for a two-level collaborative estimation scheme using spatio-temporal regularization.*** *The trajectories correspond to the low (right), and to the medium (left) layer motions.*

trajectories related to the other layers are presented in Fig.5. In the middle of the image, one can notice the estimation of two perpendicular motions : the upward motion related to sparse clouds of the intermediate layer has been accurately recovered above an underneath stratus moving downward.

6 Conclusion

In this paper, we have presented a new method for estimating winds in a stratified atmosphere from satellite image sequences. The proposed motion estimation method is based on the minimization of a functional including a two part globalized regularizer. The data term relies on shallow-water mass conservation model. Indeed, the hydrostatic assumption allows a layer decomposition of the atmosphere. This decomposition is used to derive, relatively to each layer, thickness-based observations from infrared satellite images. Resulting observations verify independent shallow-water mass conservation models. To overcome the problem of sparse observations, a robust estimator is introduced in the data term.

A novel spatio-temporal regularizer is proposed. An approximation of shallow-water momentum equations expressed in a divergence-vorticity form is used to derive temporal coherence constraints. These temporal constraints are combined with a robust second-order regularizer preserving divergent and vortic-

ity structures of the flow. In order to capture mesoscale dynamics, an optic-flow/correlation collaborative estimation scheme is proposed. Relying on two-level of estimation, this approach constitutes an advantageous alternative to the standard multiresolution framework. On both synthetic images and real satellite infrared images, the merit of the novel data-model and of the introduction of correlation-based and temporal constraints have been demonstrated.

References

1. M. Black and P. Anandan. The robust estimation of multiple motions: Parametric and piecewise-smooth flow fields. *Computer Vision and Image Understanding*, 63(1):75–104, 1996.
2. T. Corpetti, E. Mémin, and P. Pérez. Dense estimation of fluid flows. *IEEE Trans. Pattern Anal. Machine Intell.*, 24(3):365–380, 2002.
3. J. Fitzpatrick. The existence of geometrical density-image transformations corresponding to object motion. *Comput. Vision, Graphics, Image Proc.*, 44(2):155–174, Nov. 1988.
4. J. Holton. *An introduction to dynamic meteorology.* Academic press, 1992.
5. B. Horn and B. Schunck. Determining optical flow. *Artificial Intelligence*, 17:185–203, 1981.
6. J. Leese, C. Novack, and B. Clark. An automated technique for obtained cloud motion from geosynchronous satellite data using cross correlation. *Journal of applied meteorology*, 10:118–132, 1971.
7. B. Lucas and T. Kanade. An iterative image registration technique with an application to stereovision. In *Int. Joint Conf. on Artificial Intel. (IJCAI)*, pages 674–679, 1981.
8. E. Mémin and P. Pérez. Fluid motion recovery by coupling dense and parametric motion fields. In *Int. Conf. on Computer, ICCV'99*, pages 620–625, 1999.
9. P. Ruhnau, A. Stahl, and C. Schnoerr. On-line variational estimation of dynamical fluid flows with physics-based spatio-temporal regularization. In *28th Symposium of the German Association for Pattern Recognition*, Berlin, Sept. 2006.
10. J. Schmetz, K. Holmlund, J. Hoffman, B. Strauss, B. Mason, V. Gaertner, A. Koch, and L. V. D. Berg. Operational cloud-motion winds from meteosat infrared images. *Journal of Applied Meteorology*, 32(7):1206–1225, 1993.
11. D. Suter. Motion estimation and vector splines. In *Proc. Conf. Comp. Vision Pattern Rec.*, pages 939–942, Seattle, USA, June 1994.
12. A. Szantai and F. Desalmand. Using multiple channels from msg to improve atmospheric motion wind selection and quality. In *7th International Winds Workshop, EUMETSAT EUM P 42*, pages 307–314, Helsinki, Finland, June 2004.
13. A. Szantai and F. Desalmand. Basic information on msg images. fluid project 'www.fluid.irisa.fr', wp-1, report 1. Technical report, Laboratoire de Meteorologie Dynamique, 2005.
14. J. Weickert and C. Schnörr. Variational optic-flow computation with a spatio-temporal smoothness constraint. *J. Mathematical. Imaging and Vision*, 14(3):245–255, 2001.
15. J. Yuan, C. Schnoerr, and E. Memin. Discrete orthogonal decomposition and variational fluid flow estimation. *J. Mathematical Imaging and Vison*, (accepted for publication), 2006.
16. L. Zhou, C. Kambhamettu, and D. Goldgof. Fluid structure and motion analysis from multi-spectrum 2d cloud images sequences. In *Proc. Conf. Comp. Vision Pattern Rec.*, volume 2, pages 744–751, USA, 2000.